SHALLOW AND DEEP COMPACTION: A VIEW FROM THE SURFACE

Ingrid C. Kroon, Buu-Long Nguyen and Peter A. Fokker[1]
E-mail: ingrid.kroon@tno.nl

Abstract: Understanding and prediction of surface movement are both technically and socially important. Construction works, peat oxidation, clay compaction, and ground water withdrawal are shallow processes that contribute to subsidence; oil and gas production and salt mining are deep causes. We have developed an inversion procedure to disentangle the deep and shallow causes of subsidence. Our procedure employs a Bayesian inversion scheme, using forward models and other *a priori* information about the shallow and deep amount of compaction. Parameter estimation thus takes place at two different depths in the subsurface, thereby disentangling deep and shallow compaction processes causing surface movement. The uncertainty in the surface measurements and *a priori* estimates is naturally incorporated. Furthermore, spatial correlations can be taken into account through inclusion of the covariance matrix. The inversion scheme is demonstrated for some artificial cases. The first case had a compacting gas field and a compacting shallow peat layer. We demonstrate that assumptions on the subsidence bowl shape were not necessary, even when there was scatter in the data. We also show how the neglect of either deep or shallow causes of subsidence can lead to wrong results. The advantage of using the *a priori* estimates of the compaction and the covariance matrix obtained by Monte Carlo simulations is demonstrated with a second artificial example. It represented two polder areas, in which the water table was controlled to different levels. A robust solution was obtained for each polder unit, while a simpler *a priori* estimate based on the expected average clay thickness failed to reproduce the original compaction. Monte Carlo simulations can also be applied to compaction in depleting gas reservoirs. There is often knowledge available about spatial correlations, even when the absolute values of the *a priori* compaction data are quite uncertain. Then, the explicit incorporation of *a priori* known spatial correlations significantly improves the result, particularly in comparison with a general smoothness constraint (if possible).

1. Introduction

Subsidence of the surface is an important social issue in the Netherlands [1] and elsewhere [2, 3]. This is mainly due to the associated enhanced risk on flooding and on damage to buildings and infrastructure. Developments like urbanisation, intensification of subsurface use, sea level rise and more intensive rainstorms tend to increase the urgency of the issue. Reliable history matching and forecasting of surface movement is required for applications as ground water management, optimisation of hydrocarbon extraction and monitoring strategies, but also for liability issues. Current limitations in history matching and forecasting are mainly related to

[1] TNO Built Environment and Geosciences, Utrecht, The Netherlands

uncertainty in surface movement and other variables and quantification of surface movement causes. The present paper focuses at the quantification of surface movement causes.

Several natural and anthropogenic processes can result in surface movement. Some of these occur at or near the surface, like construction of buildings, roads and tunnels, oxidation of peat, clay compaction, and withdrawal of ground water. Others primarily affect the deep subsurface: earthquakes, extraction of hydrocarbons, salt tectonics and geothermal production [4]. Each process has a characteristic scale in time and space on which it affects surface movement. However, different processes may interfere or overlap in scale (Figure 1), making it difficult to distinguish them.

Inverse parameter estimation techniques have been applied to estimate reservoir compaction from surface subsidence, considering the latter as a result of reservoir depletion only [5, 6, 7]. These studies did not take into account the influence of other processes – in particular shallow compaction – on surface movement. Similarly, aquifer parameters have been estimated from surface movement, considering the latter to be the result of groundwater extraction or recharge only [8]. Neglecting either deep or shallow processes, however, may lead to erroneous reservoir parameterisation.

Our goal was to disentangle shallow and deep causes of surface movement in an objective way by solving the parameter estimation or history matching problem. Still, data uncertainty is addressed explicitly in our method.

We included forward models of both shallow and deep compaction processes. Parameter estimation thus takes place at two different depths in the subsurface, thereby disentangling deep and shallow compaction processes causing surface movement. The inverse problem of surface movement requires additional information to regularise it. Such information is usually in the form of an *a priori* parameter estimate or a spatial smoothness constraint. We used the Bayesian approach of parameter estimation, which is well established and designed to cope with these kinds of problems [9, 10]. Approaches that include single penalty and damping factors to determine the weight of the *a priori* information [11] can be seen as reduced Bayesian methods.

We present the methodology in the first part of this study. The second part shows how the algorithm was validated and tested using a number of artificial cases, and addresses the limitations of the methodology. Finally, we draw some conclusions on the applicability of the algorithm to the surface subsidence issue.

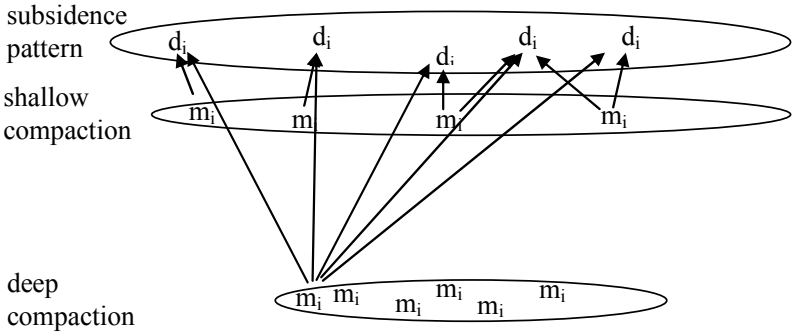

Figure 1: Sketch of shallow and deep causes of compaction (m) resulting in surface subsidence (d). Arrows denote the area of influence of individual compaction sources.

2. Methodology

2.1. Inverse model formulation

The basis of the problem can be described by:

$$\mathbf{G}(\mathbf{m}) = \mathbf{d} \tag{1}$$

m is the model parameter vector, i.e. the compaction. Both the deep and the shallow subsurface are discretised; **m** is geographically referenced on both levels. **G** is a forward model predicting the subsidence caused by both shallow and deep compaction in the locations that are associated with the measured surface movement data **d**. It is assumed that the system is linear and all component distributions are Gaussian.

We were looking for the maximum likelihood solution of **m**, provided that **d** and **G** are known. However, this problem is usually ill-conditioned or even ill-posed: with direct inversion, small variations in the measurements would cause large variations in the computed compaction. The problem is ill-posed when there are more elements in the model vector **m** than in the data vector **d**. In both cases, additional information is required to regularize the problem.

We call P(**d**|**m**) the conditional probability distribution of m given a set of data **d.** Additional information is summarized in P(**m**), the *a priori* probability distribution of **m**. P(**m**) contains information in the form of an initial model estimate <**m**> = $\mathbf{m}^0$ and a smoothness constraint. Inversion of Eq. 1 with account of the *a priori* information is then achieved by maximizing the conditional probability for **m** with given **d**, P(**m**|**d**). Following Bayes's fundamental theorem, this probability is proportional to the product of the two probabilities, P(**d**|**m**) * P(**m**). The probabilities are given by:

$$\mathrm{P}(\mathbf{d}|\mathbf{m}) * \mathrm{P}(\mathbf{m}) = \frac{e^{-\frac{1}{2}((\mathbf{Gm}-\mathbf{d})^T(\mathrm{cov}\,\mathbf{G})^{-1}(\mathbf{Gm}-\mathbf{d}))}}{\sqrt{(2\pi)^N\,|(\mathrm{cov}\,\mathbf{G})|}} * \frac{e^{-\frac{1}{2}((\mathbf{m}-<\mathbf{m}>)^T(\mathrm{cov}\,\mathbf{m})^{-1}(\mathbf{m}-<\mathbf{m}>))-\frac{1}{2}((\mathbf{Dm})^T(\mathrm{cov}\,\mathbf{D})^{-1}(\mathbf{Dm}))}}{\sqrt{(2\pi)^N\,|(\mathrm{cov}\,\mathbf{m})|}} \tag{2}$$

In this expression, N is the number of realisations, cov is short notation for covariance matrix, and **D** is a matrix containing *a priori* information on spatial correlations.

Maximising P(**d**|**m**) * P(**m**) as a function of **m** requires minimising the exponent of the resulting exponential. In the minimum, the derivative with regard to **m** is zero for every single element of the vector **m**. Differentiation and utilisation of the symmetry of the matrices C^m, C^D and C^G results (in matrix notation) in:

$$-G^T\left(C^G\right)^{-1}(\mathbf{Gm}-\mathbf{d})-(C^m)^{-1}\left(\mathbf{m}-\mathbf{m}^0\right)-D^T(C^D)^{-1}(\mathbf{Dm})=0 \tag{3}$$

Isolating the terms with m at one side of the equation and inverting the square matrix that precedes it results in the expression:

$$m=\left\{G^T\left(C^G\right)^{-1}G+(C^m)^{-1}+D^T(C^D)^{-1}D\right\}^{-1}\left\{G^T\left(C^G\right)^{-1}d+(C^m)^{-1}m^0\right\} \tag{4}$$

This is the wanted solution to the inversion problem with inclusion of the *a priori* information on the compaction model. If there is no covariance in the system, Eq. (4) simplifies to the least squares solution: $m=\left\{\sigma^{-2}{}_d G^T G+\sigma^{-2}{}_{m^0}+\sigma^{-2}{}_c D^T D\right\}^{-1}\left\{\sigma^{-2}{}_d G^T d+\sigma^{-2}{}_{m^0} m^0\right\}$. If $\sigma^{-2}{}_{m^0}$ and $\sigma^{-2}{}_c$ are constant, they are sometimes referred to as damping and penalty factor respectively (cf. Du and Olson, 2001).

2.2. Forward models

Two forward models were used. The first model describes both shallow compaction and surface subsidence due to peat oxidation. Shallow compaction can be due to lowering of aquifer head and/or lowering of groundwater level [12, 13, 14] (see also [2] and references therein). The compaction processes have both poro-elastic and inelastic effects. Irreversible compaction is likely to take place if the pre-consolidation stress is exceeded. In this study a convenient, numerically fast, 1D approach was adopted after Koppejan [15], in which compaction is described empirically. The approach has been described in more detail in Ref. [1]. Translation from layer compaction to surface subsidence was considered to be (nearly) instantaneous and primarily of local significance (Figure 1). Compaction could thus directly be interpolated to surface subsidence, provided that it occurred at shallow depth (< 50 m below surface). Peat oxidation was modelled by using a constant oxidation rate for dry peat, and taking into account the resulting decrease in (dry) peat thickness over time.

The second forward model describes the effect of a decrease in gas pressure in the reservoir during gas production. The pressure drop results in a higher effective pressure and thus in reservoir compaction. Due to the elastic properties of the overburden this compaction is usually transferred almost instantaneously to the surface, resulting in surface subsidence. However, the elasticity of the subsurface causes the subsidence to have a larger lateral extent than the compaction. The excess horizontal distance for which reservoir compaction has an influence at the surface is roughly of the same order as the depth of the reservoir (Figure 1).

The precise form of the subsidence bowl resulting from the deep compaction depends on the elastic properties of the subsurface. We used a linear, semi-analytic approach designed to account for layering. This approach employs integration of influence functions representing the subsidence bowl of a centre of compression. A centre of compression is a mathematical expression for a finite amount of compaction that is concentrated in a point. With horizontal layers only, a rotationally symmetric influence function can be constructed that applies for every deep compaction grid point, because the subsurface possesses translational symmetry. The total predicted subsidence in a point, resulting from the deep compaction, is obtained after summation over all grid blocks in the reservoir. For a comprehensive description of the construction of the influence function in a layered subsurface we refer to Ref. [16].

2.3. Inverse model algorithm

Equation 4 has been implemented in Matlab 7.0. For vector **d** the number of observations, their geographical location and variance can be chosen freely. Discretisation of **m** was done using rectangular and regular grids for shallow and deep compaction separately. Inverse distance interpolation was used for conversion between **d** and the shallow compaction grid. At every point of the compaction grids $\mathbf{m}^0$ had to be defined. Variance and covariance in $\mathbf{m}^0$ could be varied from nearly zero to infinity. For the *a priori* information on spatial correlations in D the finite difference approximation of the Laplacian operator was used. Information on the uncertainty in spatial smoothness is often only available as an order of magnitude, which makes use of one penalty factor sufficient for most applications. This factor can also be varied from nearly zero to infinity. Gauss-Jordan elimination [17] was used for the matrix inversion.

3. Model validation and testing

The inverse model algorithm has been applied to a number of artificial test cases. Synthetic subsidence data have been calculated using pre-defined compaction grids in the forward models. The extensive and fully constrained synthetic subsidence data sets were sampled in various ways, and an inversion was carried out. We have used these exercises to validate the model and to test under what conditions our inverse method is or is not capable of deriving the original compaction grids. We present a small selection of the results.

3.1. Shallow and deep compaction: a simple artificial case

The pre-defined shallow compaction grid consisted of a linearly increasing regional east-west trend (Figure 2a). In geological terms this may be considered to represent compaction of a (highly idealised) eastward thinning peat layer that pinches out at the eastern area boundary. The pre-defined deep compaction grid resembled a rectangular shaped gas reservoir with sharp boundaries (Figure 2b), as may be the case in faulted areas. The elastic properties of the subsurface were not depth averaged: a relatively strong intermediate layer was situated at depth between 2.1 and 3.0 km. The calculated surface movement (Figure 2c) was a combination of the east-west trend induced by the shallow compaction (between 0 and 0.5 m) and a subsidence bowl (with a maximum depth of -0.29 m) related to the deep compaction. Thus, in the central part of the area surface movement was controlled by shallow and deep compaction to approximately the same extent.

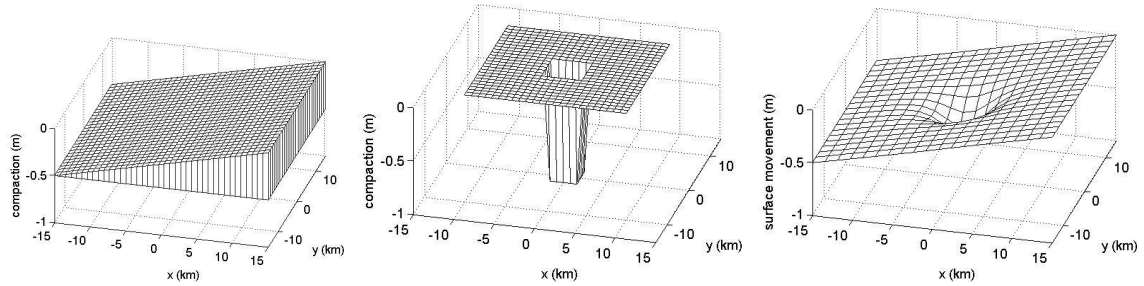

Figure 2: Forward calculation a) Shallow compaction (40x30 grid) increases linearly from 0 cm at the eastern boundary to 50 cm at the western boundary. b) Deep compaction (25x25 grid) of 1 m within the rectangular shaped reservoir. c) Resulting surface movement prediction (20x20 grid).

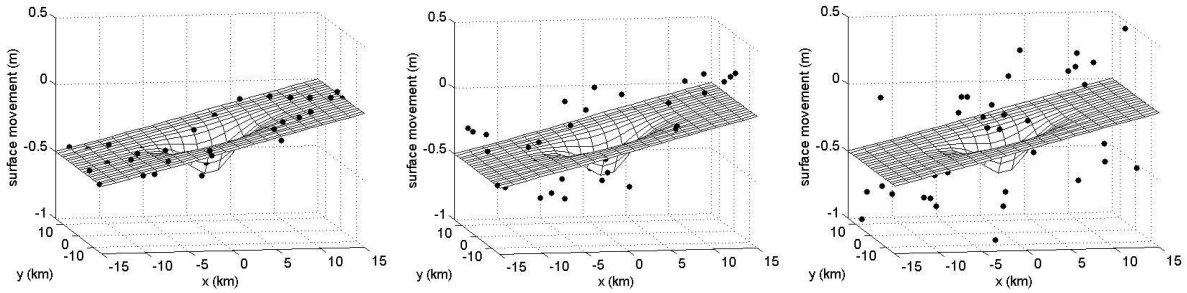

Figure 3: Synthetic subsidence data viewed from a different angle than Figure 2d. a) Subset (dots) including 10% noise ($\sigma = 0.05$) b) Subset (dots) including 50% noise ($\sigma = 0.28$) c) Subset (dots) including 100% noise ($\sigma = 0.55$).

In practice only a finite and rather small number of measurements are available to constrain the movement of the surface, and these data are often rather noisy, especially if the surface movement is relatively small. Hence, inversion was performed using only a random sample of 10% of the calculated surface movement result of the forward model (40 data points). Random noise was added progressively to the subsidence data to test the robustness of the method (Figure 3). With 10% noise, the subsidence data had a smaller variance than the initial compaction, for the tests with larger noise the variance of the subsidence was larger. The correct initial compaction models were introduced in the inversion procedure and no attempt was made to smooth the compaction models.

The results are not shown graphically, as they are similar to the input presented in Fig. 2. In the test with 10% noise the subsidence data were considered to be more reliable than the proposed initial compaction models. Hence, these compaction models were (slightly) adjusted. In this particular case this meant that they became noisier. In the other tests the subsidence data were less reliable than the proposed (correct) initial compaction models. This effectively removed (the larger part of) the introduced noise from the subsidence data. This clearly demonstrates the strength of using *a priori* information in the inversion method.

3.2. Inversion with neglect of shallow or deep compaction

The influence of shallow compaction on surface movement has to be taken into account when the surface movement above a producing or abandoned field is monitored, unless the magnitude of shallow compaction is negligibly small on the time scale of interest, or if measurements are only made at locations that are truly well founded at depth. The error created by neglecting shallow compaction is demonstrated in cases where the initial model of the deep compaction was correct, and known within different degrees of certainty. The results (Figure 4) show that – depending on the confidence in the initial model of the deep compaction – there was either a large difference between observed and estimated subsidence, or the deep compaction was substantially modified. In the first case the difference in subsidence displayed a clear east-west trend. Such a clear and deviating trend may serve as a warning that a significant process (shallow compaction) has been neglected. If on the other hand the initial deep compaction model was assumed very uncertain, this effect was small, whereas estimated deep compaction did extend well beyond expected reservoir boundaries and displayed a clear east-west trend: subsidence that was caused by shallow compaction was now attributed erroneously to deep compaction.

Naturally, any unexpected source of deep compaction (e.g. aquifer support, compaction in Tertiary clays, natural depletion of a deep aquifer after a faulting event) will also influence inversion of shallow compaction. The error created by neglecting deep compaction can be demonstrated for the case where the initial model of the shallow compaction is correct, but is known within different degrees of certainty. The additional subsidence in the data is corrected for locally, unless a certain smoothness of the shallow compaction is assumed. Then the deviation has in fact the shape of a bowl. Thus, subsidence caused by deep compaction is now attributed erroneously to shallow compaction.

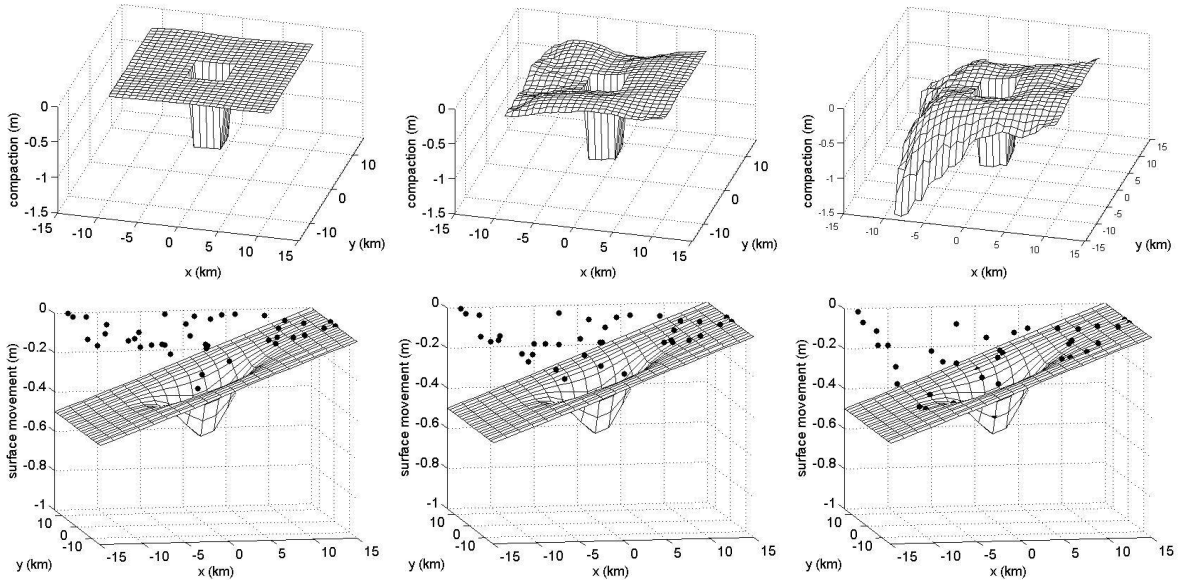

Figure 4: Inverse calculation results assuming only deep compaction a) Best estimate of deep compaction for a σ^2 of the initial deep compaction of 0.01, 0.1 and 1 respectively. b) Original subsidence data (mesh) and the best estimate of the subsidence (dots) based on forward modelling using the deep compaction estimates shown in (a).

3.3. Inversion using Monte Carlo simulation

Here a more complex artificial case of shallow compaction is introduced (Figure 5a). At the start the model had an initially flat surface at 0 m and was 5 m thick. It was divided into two polder units, separated along a sharp east-west boundary (the dike). At the bottom of the model an aquifer was present with an hydraulic head of 0.5 m above surface. The northern polder unit had an initial phreatic level of -0.8 m below the surface, whereas the southern polder had an initial phreatic level of -0.5 m below the surface. After 5 years, the phreatic level in both polders was lowered by 0.2 m and the hydraulic head of the aquifer was lowered by 0.1 m. In total 15 years were modelled. The subsurface consisted of peat that was covered by a layer of clay. At one boundary the clay thickness was 0.5 m, the opposite boundary had a clay thickness of 0.24 m. The resulting subsidence movement was resampled to provide a random set of subsidence data (40 data points; Figure 5b). This set was used as input in the inversion.

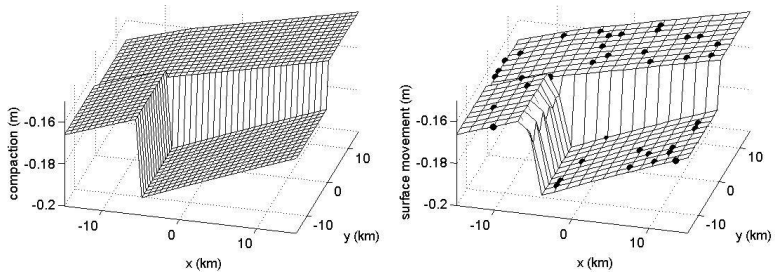

Figure 5: Forward calculation. a) Shallow compaction (40x30 grid) of 1 particular realisation in which clay thickness decreases from 0.5 m to 0.24 m. b) Resulting surface movement prediction (20x20 grid). Subset (dots) on which inversion will be based.

In the inversion it was assumed that the set up of the model was known. However, clay thickness was highly uncertain at the second boundary: it could be between 0 en 1 m thick (it was 0.24 m). A Monte Carlo simulation (50 realisations) was performed in order to derive *a priori* estimates of (median) shallow compaction, variance and covariance for every grid point as a function of the uncertainty in clay thickness. Alternatively, one could choose to simply use the realisation of the expected average clay thickness of 0.5 m as the *a priori* estimate and then allow for a large variance in the model. Due to the known presence of abrupt, artificial boundaries between polder units, use of a blind smoothing constraint is not justified in either case.

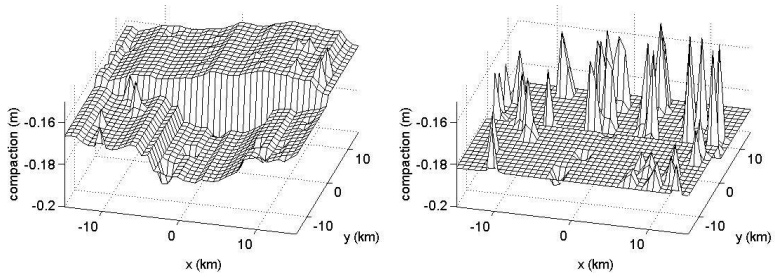

Figure 6: Inverse calculation results a) Best estimate of shallow compaction using the median of the Monte Carlo simulation and the corresponding covariance matrix. b) Best estimate of shallow compaction using average clay thickness of 0.5 m with a constant variance of $1*10^{-3}$ m^2.

Inversion results of both alternatives are shown in Figure 6. Clearly, inversion using the Monte Carlo results approached the original compaction (Figure 5a) best. Differences reflect the high amount of uncertainty and scarcity of data points. The result is remarkably smooth given the absence of a smoothness constraint. This is partly due to the reasonable *a priori* estimate and partly due to the introduction of non-zero covariances. The non-zero covariance quantifies expected relations between grid points. In this particular case the grid points were sharing the same groundwater regime or had a similar clay cover thickness. In effect, each data point (partially) updated all other grid points with which it shared a non-zero covariance. On the other hand, simply using average clay thickness in combination with a high variance did produce a lot of spikes and completely failed to reproduce the abrupt change in compaction in one of the polder units (Figure 6b).

Hence, it is worthwhile to use Monte Carlo simulations for defining *a priori* estimates. The explicit use of the covariance can be particularly advantageous in optimisation problems: adding only a few more data points at carefully chosen locations sharing a high covariance with many other grid points and/or grid points of interest will significantly improve the solution constraints.

4. Conclusions

We have created and tested a Bayesian inversion scheme that disentangles deep and shallow causes of subsidence. Assumptions on the shape of the subsidence bowl are not necessary, even when there is considerable uncertainty in the measurements. The shape of the subsidence bowl is a result of the inversion procedure, and the knowledge about the subsurface is incorporated at its most basic level: the shape of the reservoirs and the expected compaction behaviour.

When the contributions of deep and shallow compaction to the subsidence have a similar order of magnitude, the neglect of one of them leads to wrong conclusions. This has been demonstrated using a realistic artificial example.

Instrumental in the procedure is the use of proper *a priori* information and spatial correlations. This information has been introduced in the covariance matrix. A possible method to establish this matrix is through Monte Carlo simulations. In such simulations, proper attention must be given to the forward models as they have a significant influence on the quality of the final result. A second artificial example has shown the added value of the use of Monte Carlo simulations and their results for the *a priori* estimates of the compaction, and its variance and covariance.

Monte Carlo simulations can also be applied to compaction in depleting gas reservoirs. There is often knowledge available about spatial correlations, even when the absolute values of the *a priori* compaction data are quite uncertain. Then, the explicit incorporation of *a priori* known spatial correlations significantly improves the result, particularly in comparison with a general smoothness constraint.

The method is suitable for monitoring reservoir behaviour and depletion zones lacking pressure measurements, such as lateral aquifers or undrilled reservoir blocks. These two applications were put forward by Marchina [5]. However, our method can also be applied in areas where the subsidence signal of reservoir depletion is distorted by unrelated shallow compaction.

References

[1] Bremmer, C.N., Lange, G. de, Linden, W. van der, Veling, E., Veldkamp, J.G. (2003) *Bodemdaling en Integraal Waterbeheer* (Subsidence and Integrated Water Management). Final report Delft Cluster Project 06.03.02. TNO-NITG report 03-200-A.

[2] Schmidt, D.A., Bürgmann, R. (2003) Time-dependent land uplift and subsidence in the Santa Clara valley, California, from a large interferometric synthetic aperture radar data set. J. Geophysical Research 108, B9, 2416, p. 13

[3] Holzer, Thomas L. and Devin L. Galloway (2005) Impacts of land subsidence caused by withdrawal of underground fluids in the United States, Reviews in Engineering Geology XVI (Geological Society of America), 87 – 99.

[4] Carnec, C., Fabriol, H. (1999) Monitoring and land subsidence at the Cerro Prieto geothermal field, Baja California, using SAR interferometry. Geophysical Research Letters, 26, 1211-1214

[5] Marchina, P.J.M. (1996) The use of subsidence data to monitor reservoir behaviour. SPE paper 36918, presented at the 1996 SPE European Petroleum Conference, Milan, Italy.

[6] Vasco, D.W., Karasaki, K., Doughty, C. (2000) Using surface deformation to image reservoir characteristics. Geophysics 65, 132-147

[7] Du, J., Olson, J.E. (2001) A poroelastic reservoir model for predicting subsidence and mapping subsurface pressure fronts. J. Petroleum Sci. Engineering 30, 181-197

[8] Pavelko, M.T. (2004) Estimates of hydraulic properties from a one-dimensional numerical model of vertical aquifer-system deformation, Lorenzi Site, Las Vegas, Nevada. U.S.G.S. Water-Resources Investigations Report 03-4083, p. 35

[9] Menke, W. (1989) Geophysical data analysis: Discrete inverse theory. International Geophysics Series vol. 45, 289 p.

[10] Parker, R.L. (1994) Geophysical inverse theory: Princeton Univ. Press
[11] Du, Y., Aydin, A., Segall, P. (1992) Comparison of various inversion techniques as applied to the determination of a geophysical deformation model for the 1983 Borah Peak earthquake. Bull. Seismol. Soc. America vol. 82, no. 4, 1840-1866
[12] Schothorst, C.J. (1977) Subsidence of low moor peat soils in the Western Netherlands. Geoderma 17, 265-291.
[13] Beuving, J., Van den Akker, J. J. H., 1996, *Maaiveldsdaling van veengrasland bij twee slootpeilen in de polder Zegvelderbroek*, (Surface subsidence of peat meadow land at two surface water levels in the polder Zegvelderbroek), Staring Centrum, Instituut voor Onderzoek van het Landelijk Gebied, SC-DLO rapport 377, Wageningen.
[14] Lu, Z., and W. Danskin, (2001) InSAR analysis of natural recharge to define structure of a ground-water basin, San Bernardino, California, Geophysical Research Letters, 28, 2661-2664.
[15] Koppejan, A. W. (1948) A formula combining the Terzaghi load-compression relationship and the Buisman secular time effect*, Proc. 2nd Int. Conf. Soil Mechs. and Found. Engng.,* Part 3, Rotterdam, p. 32-37
[16] Fokker, P.A., Orlic, B. (2006, in press) Semi-analytic Modelling of Subsidence. Mathematical Geology
[17] Press, W.H., Flannery, B.P., Teucholsky, S.A.., Vetterling, W.T. (1987) Numerical recipes. The art of scientific computing. Cambridge University Press, U.S.A.